

PAPER

Room-temperature electric field modulation of magnetization in a helimagnet

To cite this article: Zhipeng Yu *et al* 2020 *J. Phys. D: Appl. Phys.* **53** 025001

View the [article online](#) for updates and enhancements.



IOP | ebooks™

Bringing you innovative digital publishing with leading voices to create your essential collection of books in STEM research.

Start exploring the collection - download the first chapter of every title for free.

Room-temperature electric field modulation of magnetization in a helimagnet

Zhipeng Yu¹, Yizhi Zhang², Kun Zhai^{1,5}, Chao Liu¹, Anmin Nie^{1,5}, Na Su³, Jinguang Cheng^{3,4}, Fusheng Wen¹, Jianyong Xiang¹, Congpu Mu¹, Bochong Wang¹, Hongtao Wang², Yongjun Tian¹ and Zhongyuan Liu^{1,5}

¹ Center for High Pressure Science (CHiPs), State Key Laboratory of Metastable Materials Science and Technology, Yanshan University, Qinhuangdao 066004, People's Republic of China

² Institute of Applied Mechanics, Zhejiang University, Hangzhou, 310027, People's Republic of China

³ Beijing National Laboratory for Condensed Matter Physics, Institute of Physics, Chinese Academy of Sciences, Beijing 100190, People's Republic of China

⁴ Songshan Lake Materials Laboratory, Dongguan, Guangdong 523808, People's Republic of China

E-mail: kunzhai@ysu.edu.cn, anmin@ysu.edu.cn and liuzy0319@ysu.edu.cn

Received 16 August 2019, revised 1 October 2019

Accepted for publication 10 October 2019

Published 29 October 2019



Abstract

Room-temperature electric field control of magnetization is of interest for the potential application of low consumption nonvolatile memory. Here, we report the realization of electric field modulation of magnetization in a single phase multiferroic material $\text{Ba}_{0.5}\text{Sr}_{1.5}\text{Co}_2\text{Fe}_{11}\text{AlO}_{22}$. In this work, we use static and dynamic measurements to reveal the magnetoelectric coupling between magnetization (M) and polarization (P). At the temperature of 10 K, the first order magnetoelectric (ME) term is dominated and the magnetization linearly changes with the electric field. While at room temperature, the quadratic term become apparent, leading to symmetric butterfly-like P - H and M - E curves. Our study reveals that an alternating longitudinal conical (ALC) phase induced exchange interaction may exist in Y type hexaferrite $\text{Ba}_{0.5}\text{Sr}_{1.5}\text{Co}_2\text{Fe}_{11}\text{AlO}_{22}$ and contribute to the ME coupling mechanism.

Keywords: multiferroics, magnetoelectric effect, hexaferrite

Supplementary material for this article is available [online](#)

(Some figures may appear in colour only in the online journal)

The cross coupling between magnetization (M , spin) and polarization (P , charge) in intrinsic or artificial ME materials provide new dimension for designing novel functionalities [1–5]. Especially, the controlling of magnetism by electric field attracts broad interest in fabricating novel ME or spintronic devices due to the reduction of Joule heating by using voltage instead of electrical current [4, 6–8]. The electric field modulating of magnetization can be realized in a variety of real systems, such as strain mediated magnetization in composite ME heterostructures [9–15], electrochemical effects modulated interfacial magnetism in low dimensional material [16–18] or direct charge-spin correlated single phase multiferroics [19, 20]. The coupling between polarization and

magnetism in multiferroics of spin origin is originated from inverse Dzyaloshinskii–Moriya (DM) mechanism or spin current model ($P \sim \sum \mathbf{e}_{12} \times (\boldsymbol{\mu}_2 \times \boldsymbol{\mu}_1)$) [21], p-d hybridization ($P \sim \sum \mathbf{e}_1 (\mathbf{e}_1 \cdot \boldsymbol{\mu}_1)^2$) [22] and exchange striction interaction ($P \sim \prod \boldsymbol{\mu}_1 \cdot \boldsymbol{\mu}_2$) [23]. Different from the composite ME materials, the single phase multiferroics can intrinsically manipulate bulk magnetization by electric field, which would have simple structure in fabricating devices [24]. E induced variation of M have been realized in some single-phase bulk materials, such as $R\text{FeO}_3$ ($R = \text{Dy}_{0.70}\text{Tb}_{0.30}$, $\text{Dy}_{0.75}\text{Gd}_{0.25}$) [25], $\text{Fe}_2\text{Mo}_3\text{O}_8$ [26], Ni_3TeO_6 [27] and so on. However, the ME effect in these single phase materials can rarely be preserved to room temperature.

Hexaferrites with tunable conical magnetic structure demonstrate prominent ME effect, especially the property

⁵ Author to whom any correspondence should be addressed.

of electric field controlling magnetization [28]. Hexaferrites can be classified into different types by the stacking sequence of T ((Ba, Sr)₂Fe₈O₁₄), R ((Ba, Sr)Fe₆O₁₁), S (Me²⁺Fe₄O₈) building blocks, consisting of M type hexaferrite (Ba, Sr)Fe₁₂O₁₉, Y-type hexaferrite (Ba, Sr)₂Me₂Fe₁₂O₂₂, Z type (Ba, Sr)₃Me₂Fe₂₄O₄₁ and U-type hexaferrite (Ba, Sr)₄Me₂Fe₃₆O₆₀ (stacking sequence: RSR*S*, TSTSTS, RSTSR*S*T*S* and RSR*S*TS*, respectively) [28–34]. In particular, highly Sr doped Z type hexaferrite (space group: *P*₆/*mmm*) and Y type hexaferrites (space group: *R*-3*m*) with specific chemical composition can display the ME effects up to room temperature. A recent symmetry-based analysis has shown that the *P*-*M* clamping mechanism of *p*-*d* hybridization is prominent in Z type hexaferrite and the non-reversal of polarization (butterfly shape) can be induced [35]. In contrast, due to the constrain by the symmetry of Y type hexaferrites, electric polarization reverses with magnetic field inducing the apparently linear ME effect, where only inverse Dzyaloshinskii–Moriya interaction works.

Here, we report the room temperature *E* control of *M* in Y type hexaferrite Ba_{0.5}Sr_{1.5}Co₂Fe₁₁AlO₂₂. We use ME current measurements, static voltage control of magnetization method and dynamic ME coefficient measurements to reveal the ME coupling. Ba_{0.5}Sr_{1.5}Co₂Fe₁₁AlO₂₂ shows a linearly electric field manipulating of magnetization in the low temperature and quadratic ME effect at high temperature. The Ba_{0.5}Sr_{1.5}Co₂Fe₁₁AlO₂₂ with room temperature noncollinear *E* control of *M* effect can be used as a candidate of ME coefficient based nonvolatile random memory.

The sample of polycrystalline Y type hexaferrite Ba_{0.5}Sr_{1.5}Co₂Fe₁₁AlO₂₂ was synthesized via solid-state reaction. High purity powders of BaCO₃ (99%, Alfa Aesar), SrCO₃ (99%, Alfa Aesar), Co₃O₄ (99.9%, Alfa Aesar), Fe₂O₃ (99.9%, Alfa Aesar), Al₂O₃ (99.9%, Alfa Aesar) were weighted to the desired chemical composition and mixed by a mortar. The mixer was calcinated at 1100 °C in furnace for several hours. Then it was pressed into a cylinder shape and synthesized at 1200 °C for 20h. The as-grown sample was polished to a thin plate for electrical measurements. To elevate the insulating properties of the sample, the thin plate was annealed in 10 atm O₂ atmosphere for 10h. The phase purity of obtained polycrystalline sample was examined by x-ray diffraction (Smartlab, Rigaku). The chemical compositions of Ba_{0.5}Sr_{1.5}Co₂Fe₁₁AlO₂₂ were examined via EDX elemental maps, a probe aberration corrected FEI Themis Z 300 TEM, equipped with Super X EDX system. The magnetization was measured at the physical property measurement system (PPMS, EverCool, Quantum Design) equipped with vibrating sample magnetometer (VSM). A homemade VSM sample holder was used to perform the electric field modulating of magnetization (figure S1 (stacks.iop.org/JPhysD/53/025001/mmedia)). The dielectric and ME currents measurement were carried out in PPMS using a inductance-capacitance-resistance (LCR) meter (Agilent E4980A) and a high resistance current meter (Keithley 6517B). The ac voltage for dielectric measurement is 1 V with *f* = 500 kHz. The electric polarization was obtained by integrating the ME current with time. Before magnetoelectric current and *M*-*E* curve measurements, the ME annealing

procedures were conducted as follows: Set magnetic field to 50 kOe, then perform an electric field perpendicular to *H*. *H* was subsequently ramped to 5 kOe to obtain an aligned ME domain state. Turn off the electric field and the electrodes were shorted for about 30 min to obtain background current below 1 pA. The dynamic ME coefficients α_E were measured by a lock in amplifier (SR830) synchronized with an ac current source (Keithley 6221) providing ac current to the solenoid to generate a small ac magnetic field *h* = 2 Oe at *f* = 1 kHz (See figure S2 for the magnetoelectric susceptibility measurement setup and principle).

Figure 1(a) demonstrate the crystal structure of Y-type helimagnet Ba_{0.5}Sr_{1.5}Co₂Fe₁₁AlO₂₂(BSCFAO). The crystal structure can be classified into two different magnetic blocks (large magnetic moment blocks (L blocks) and small magnetic moment blocks (S blocks)) distinguished by two different colors in figure 1(a). Figure 1(b) shows the elemental distribution of BSCFAO obtained by energy dispersive x-ray (EDX), which confirms a uniform distribution of chemical element Ba, Sr, Co, Fe, Al, O. The characterized XRD pattern was shown in figure 1(c) and the peak positions correspond well to the calculated XRD peaks, which demonstrate the single-phase nature of the sample. The electric polarization is generated by the noncollinear magnetic structure in Y-type hexaferrite BSCFAO due to the inverse Dzyaloshinskii–Moriya (D–M) interaction induced atomic displacement (equivalent with spin current model) [22]. Particularly, the longitudinal cone (LC) structure is essential in producing electric polarization. The *c* component arrangements of L and S magnetic moments lead to two spin configurations: ferrimagnetically aligned normal longitudinal cone (NLC) and antiferromagnetically arranged alternating longitudinal cone (ALC) (figure 1(d)). Typically, with magnetic field along *ab* plane, the electric polarization can be generated perpendicularly to *H*. In fact, in ALC magnetic structure, the *c*-axis magnetic moment component can form ‘↑↑ ↓ ↓’ spin sequence and the exchange striction interaction hide in the *P*-*M* clamping mechanism [36, 37].

Figure 1(e) shows the temperature dependence of magnetization in a wide increasing temperature range from 2 K to 800 K after *H* = 500 Oe field cooling procedures. The sample enters into magnetic order state at the temperature of 730 K (*T*_C). With decreasing temperature, a few step-like features are visible until a cusp anomaly can be observed in the *M*-*T* profiles around 430 K (*T*₁), signifying the formation of noncollinear magnetic structure. In the related compounds, such as Ba_{0.3}Sr_{1.7}Co₂Fe₁₁AlO₂₂ [36], BaSrCo₂Fe₁₁AlO₂₂ [37], Ba_{0.5}Sr_{1.5}Zn₂(Fe_{0.92}Al_{0.08})₁₂O₂₂ [38], the neutron diffraction data show a commensurate peak intensity at (1 0 1) below *T*₁, which represents the antiferromagnetically arrangement of moments in *c* axis, an indication of ALC phase. The similar noncollinear ALC magnetic structure may stabilize in our compound and the ME effect at room temperature can be expected. Then electrical measurements were performed to verify its ME effect.

Figure 2(a) demonstrate the magnetic hysteresis loop at different temperatures and figure 2(b) show the relative dielectric constant dependence on magnetic field of BSCFAO at 10 K to 300 K (see figure S3 for more details about the

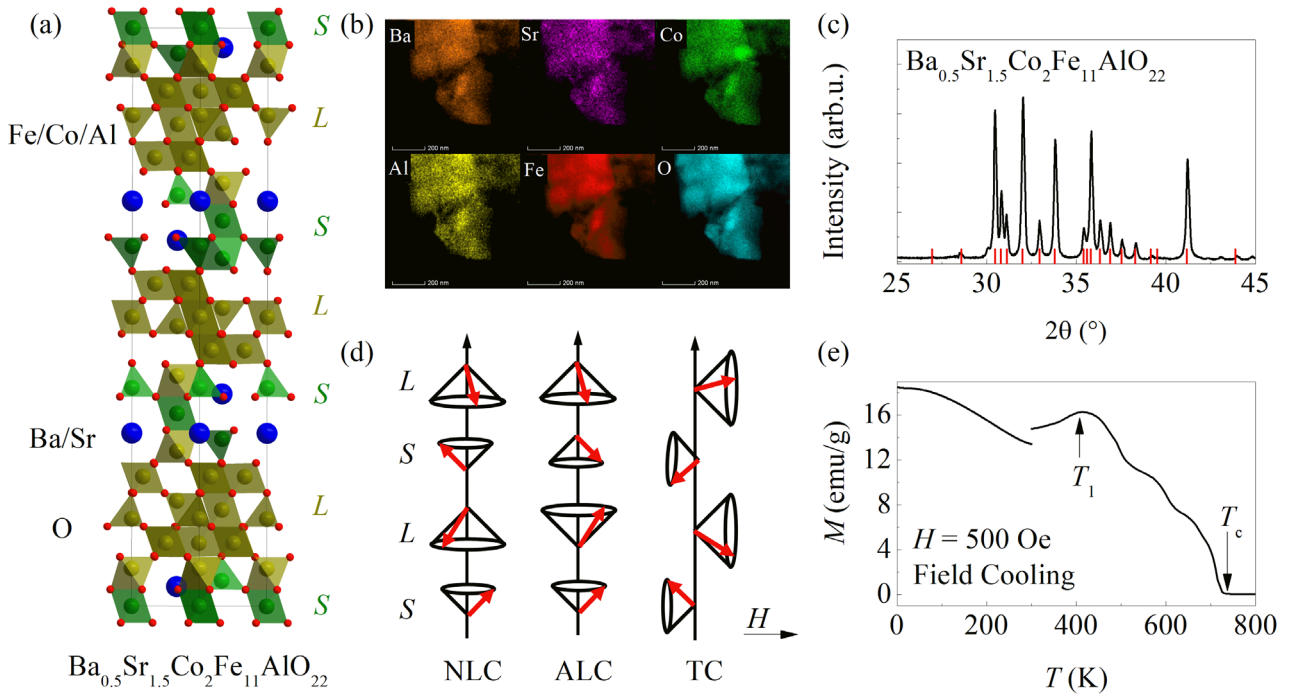


Figure 1. (a) The crystal structure of Y-type hexaferrite $\text{Ba}_{0.5}\text{Sr}_{1.5}\text{Co}_2\text{Fe}_{11}\text{AlO}_{22}$. The yellow part represents *S* magnetic block and the green part represent *L* magnetic block. Fe/Co/Al occupy tetrahedra and octahedral sites randomly. (b) The EDX elemental maps of $\text{Ba}_{0.5}\text{Sr}_{1.5}\text{Co}_2\text{Fe}_{11}\text{AlO}_{22}$. (c) The XRD pattern of synthesized Y-type hexaferrite $\text{Ba}_{0.5}\text{Sr}_{1.5}\text{Co}_2\text{Fe}_{11}\text{AlO}_{22}$. The red vertical lines represent the calculated peak positions (d) The schematic illustration of magnetic cones. (e) The temperature dependence of magnetization from 2 K to 800 K with $H = 500$ Oe.

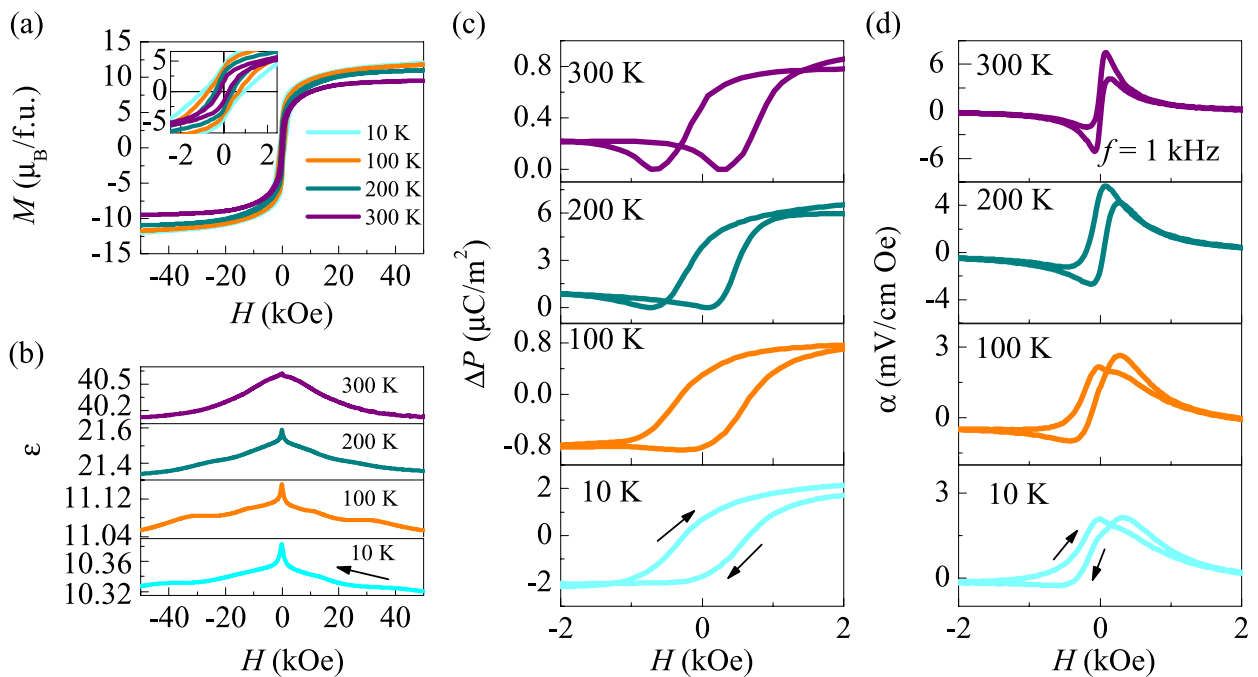


Figure 2. (a) The $M-H$ hysteresis loop at 10 K–300 K (b) the ϵ dependence of magnetic field at different temperatures. The arrow denotes the direction of changing magnetic field. The dielectric measurement stimuli ac voltage is 1 V at the frequency of 500 kHz. (c) The ΔP change with magnetic field range of -2 kOe to 2 kOe at 10 K, 100 K, 200 K, 300 K. (d) The dynamic ME coefficient at the field range of -2 kOe to 2 kOe at 10 K, 100 K, 200 K, 300 K.

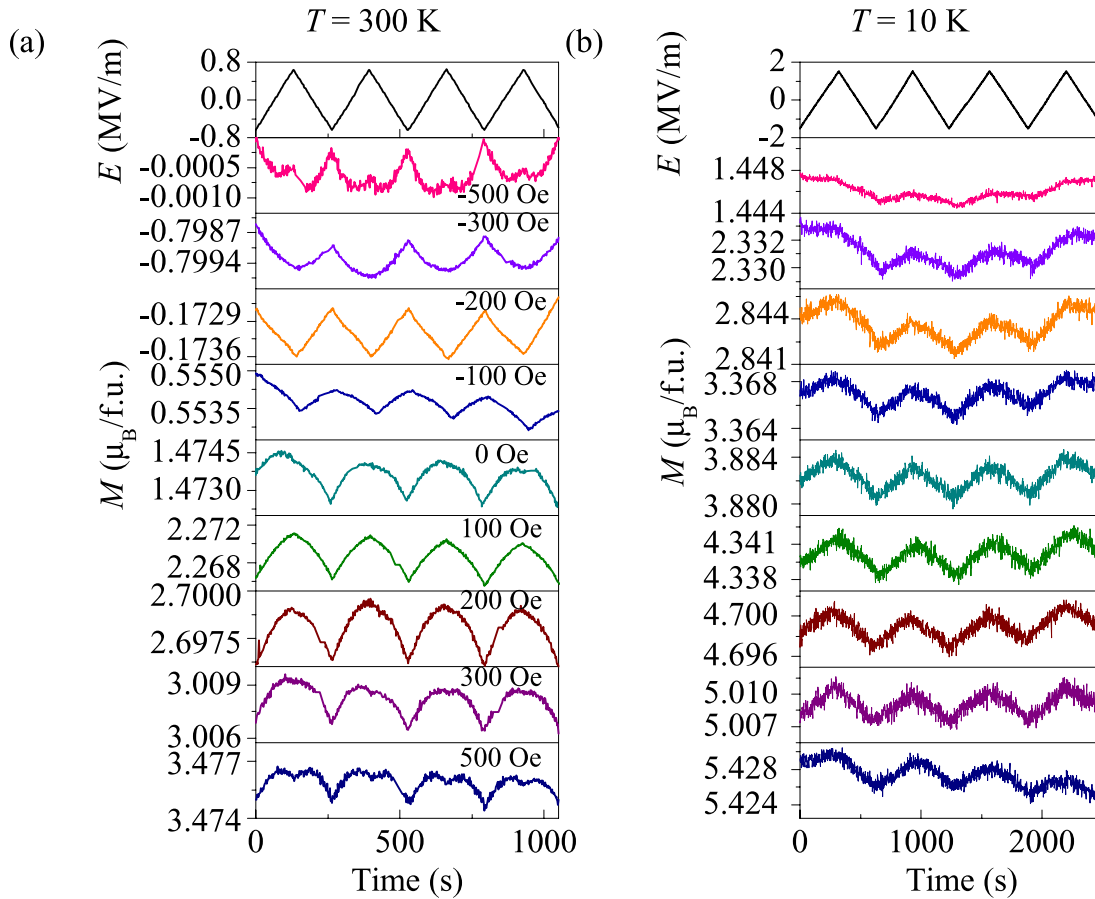


Figure 3. The periodical modulation of magnetization as a function of time at (a) 300 K and (b) 10 K under different bias magnetic field after $+E$ & $+H$ poling history.

magnetodielectric curves). At 300 K, the resistance of the sample is about $236 \text{ M}\Omega$ (the electrical resistivity is about $4.89 \times 10^8 \Omega \cdot \text{cm}$), which leaky current signal may be included in the dielectric measurements. While at low temperature, the resistance is over $\text{G}\Omega$ and the magnetoresistance effect can be excluded from the magnetodielectric measurements (see figure S4 for the resistance measurement). In figure 2(c), the $\Delta P-H$ curve exhibits apparent butterfly shape at 300 K and 200 K, similar to Z type hexaferrites, where the quadratic term is apparent [32, 34]. The maximum polarization is 0.8 and $6.5 \mu\text{C m}^{-2}$, respectively. When temperature down to 100 and 10 K, an odd function-like hysteresis $P-H$ loop shows up, indicating the dominant linear ME effect (Refer to figure S5 for the corresponding ME current at different temperatures). Further measurements of dynamic coefficient α were shown in figure 2(d). At 300 K, the ME coefficient α_E as a function of magnetic field displays a peak-dip feature (consistent with the derivation of P by H at 300 K) evidencing the strong second order $M-E$ coupling. The maximum ME coefficient is $7.5 \text{ mV (cm Oe)}^{-1}$ located at $H = 100 \text{ Oe}$. At 200 K, the shape of the curve is preserved and the maximum ME coefficient is reduced to $5.4 \text{ mV (cm Oe)}^{-1}$. Upon decreasing temperature down to $T = 100$ and 10 K, the dip of the α_E-H curve is not obvious when sweeping the magnetic field from $+2 \text{ kOe}$

to -2 kOe . While the dip still shows up once sweeping the magnetic field from the opposite direction -2 kOe to $+2 \text{ kOe}$, which may attribute to different domain state. We can see that the quadratic ME effect is obvious at room temperature, but is diminished at low temperatures.

Then the magnetization under electric field was performed. We firstly set the magnetic field to 50 kOe and apply an electric field ($E = 0.7 \text{ MV m}^{-1}$ @ 300 K and $E = 1.5 \text{ MV m}^{-1}$ @ 10 K) to the sample to align domains, where E perpendicular to H . Figure 3(a) shows the magnetization periodically modulating with continuous electric field under different magnetic fields at 300 K. At 500 Oe to 0 Oe, the magnetic moment and electric field change in the same direction. When $H = -100 \text{ Oe}$, in the vicinity of coercive field, the magnetization reverse to $-M$, which induces the ‘negative’ correlation between magnetization and electric field (Also seen in figures S6 and S7 in $-E&H$ poling condition). At 10 K, the magnetization almost linearly varies with applied electric field at different bias H in the range of -500 Oe to 500 Oe .

In order to have a straight comparison, the $M-E$ curves are further shown in figures 4(a) and (b). At 300 K, the magnetization curve nonlinearly changes with electric field with the maximum modulation of magnetization reaching $2.21 \times 10^{-4} \mu_B/\text{f.u.}$ at $H = 100 \text{ Oe}$. At higher positive or

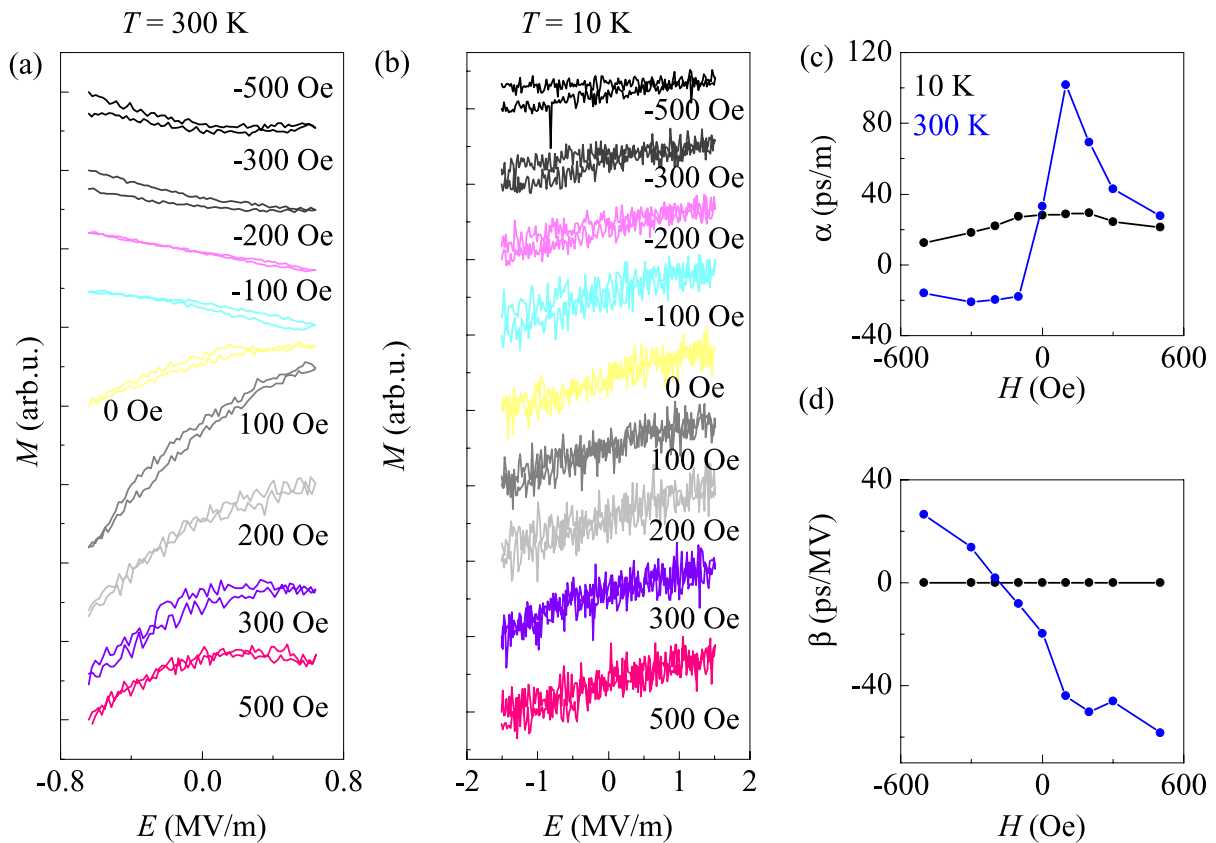


Figure 4. The electric field modulation of magnetization at (a) 300 K and (b) 10 K under different magnetic field. The calculated (c) first order ME coefficient α and (d) second order ME coefficient β variation with external magnetic field.

negative magnetic field, the curves bend more, leading to the appearance of quadratic term under magnetic field. In contrast, as shown in figure 4(b), the M - E curves linearly changed at 10 K at different H . The variations of M by E can be effectively expressed by the equation $\mu_0 M = \alpha E + \beta E^2$ (α is the linear converse ME coefficient and β is the quadratic converse ME coefficient) [7]. By fitting the increasing and decreasing branches of E - M curves under external magnetic field via this equation, the average α (β) dependence of H was summarized in figures 4(c) and (d). The maximum linear converse ME coefficient α_C increases with decreasing H (in the direction of 500 Oe to -500 Oe) and reach the maximum value (101 ps m^{-1}) at $H = 100$ Oe. With further increasing H , the α_C sharply decreases and reach negative value at $H = -100$ Oe. The peak-dip feature of calculated α_C - H curve is consistent with the dynamic ME coefficient dependence on H shown in figure 2(c). The calculated converse ME coefficients at 10 K are smaller than those at 300 K and α_C - H curve is also resemble the dynamic ME coefficient curve in figure 2(d). The second order ME coefficient β at 10 K and 300 K were shown in figure 4(d). From $H = 500$ Oe to $H = -500$ Oe, β almost linearly changes from negative value to positive value, except the anomalies at $H = 100$ and 200 Oe. As shown in the inset, the value of β at $T = 10$ K is at the orders of $10^{-2} \text{ ps MV}^{-1}$, greatly smaller than that at 300 K, evidencing the linear ME effect nature in low temperature. The calculated α and β at room temperature after $-E$ & H poling condition was shown in figure S7.

Form above, we find P - H (M - E) curves of Y type hexaferrite BSCFAO are similar to Z type hexaferrite at room temperature (non-reversal feature), contradict with symmetry analysis in previous study, which may indicate an additional mechanism existing in highly Sr doped Y-type hexaferrite BSCFAO. According to previous study in $E \perp H$ configuration, the in plane magnetic cone rotation under H reverses the spin helicity and electric polarization spontaneously reverses. While the out of plane cone rotation keeps the sign of polarization [30]. The peak-dip feature of the ME coefficient dependence on H at high temperature in our study indicate the possibility of out of plane cone rotation and the ALC phase can be generated. Similarly, obtained by the neutron diffraction data, the related compound $\text{BaSrCo}_2\text{Fe}_{11}\text{AlO}_{22}$, $\text{Ba}_{0.3}\text{Sr}_{1.7}\text{Co}_2\text{Fe}_{11}\text{AlO}_{22}$ [36, 37] show ALC phase at low magnetic field and a hidden ' $\uparrow\uparrow\downarrow\downarrow$ ' magnetic structure exists along c axis. Based on the noncollinear ME effect, an ALC phase induced exchange striction interaction may responsible for the even-function like ME effect in our case at high temperature.

In conclusion, we have thoroughly studied the ME effect in a Y type hexaferrite $\text{Ba}_{0.5}\text{Sr}_{1.5}\text{Co}_2\text{Fe}_{11}\text{AlO}_{22}$. In particular, the room temperature E modulation of M is realized in this compound with the highest converse ME coefficient 101 ps m^{-1} . Furthermore, both the dynamic and static measurements present a linear ME effect at low temperature and a noncollinear ME effect at high temperature, which may come from different magnetic structures and an extra exchange striction interaction play a role in P - M clamping.

Acknowledgments

This work was supported by the National Natural Science Foundation of China (Grant No. 51732010) K Z also appreciate a startup grant from Yanshan University (No. BL18058). J G C is supported by MOST, NSFC, and CAS (Grant Nos. 2018YFA0305700, 11574377, 11834016, 11874400, and QYZDB-SSW-SLH013).

Conflicts of interest

There are no conflicts to declare.

ORCID iDs

Kun Zhai  <https://orcid.org/0000-0002-1465-6778>
 Jinguang Cheng  <https://orcid.org/0000-0002-4969-1960>
 Fusheng Wen  <https://orcid.org/0000-0002-6827-5348>
 Jianyong Xiang  <https://orcid.org/0000-0001-9374-7127>
 Congpu Mu  <https://orcid.org/0000-0003-1656-716X>
 Bochong Wang  <https://orcid.org/0000-0001-5801-5369>

References

- [1] Eerenstein W, Mathur N D and Scott J F 2006 *Nature* **442** 759
- [2] Fiebig M, Lottermoser T, Meier D and Trassin M 2016 *Nat. Rev. Mater.* **1** 16046
- [3] Spaldin N A and Ramesh R 2019 *Nat. Mater.* **18** 203–12
- [4] Shen J, Cong J, Chai Y, Shang D, Shen S, Zhai K, Tian Y and Sun Y 2016 *Phys. Rev. Appl.* **6** 021001
- [5] Manipatrunil S, Nikonov D E, Lin C-C, Gosavi T A, Liu H, Prasad B, Huang Y-L, Bonturim E, Ramesh R and Young I A 2019 *Nature* **565** 35–42
- [6] Jiang S, Shan J and Mak K F 2018 *Nat. Mater.* **17** 406–10
- [7] Zhai K et al 2017 *Nat. Commun.* **8** 519
- [8] Matsukura F, Tokura Y and Ohno H 2015 *Nat. Nanotechnol.* **10** 209–20
- [9] Cherifi R O et al 2014 *Nat. Mater.* **13** 345
- [10] Lee Y et al 2015 *Nat. Commun.* **6** 5959
- [11] Liu Z Q et al 2016 *Phys. Rev. Lett.* **116** 097203
- [12] Clarkson J D et al 2017 *Sci. Rep.* **7** 15460
- [13] Fina I, Quintana A, Martí X, Sánchez F, Foerster M, Aballe L, Sort J and Fontcuberta J 2018 *Appl. Phys. Lett.* **113** 152901
- [14] Chen A et al 2019 *Nat. Commun.* **10** 243
- [15] Dong G et al 2017 *ACS Appl. Mater. Interfaces* **9** 30733–40
- [16] Molinari A, Hahn H and Kruk R 2018 *Adv. Mater.* **30** 1703908
- [17] Tan A J, Huang M, Avci C O, Büttner F, Mann M, Hu W, Mazzoli C, Wilkins S, Tuller H L and Beach G S D 2019 *Nat. Mater.* **8** 35–41
- [18] Lu N et al 2017 *Nature* **546** 124–8
- [19] Hirose S, Haruki K, Ando A and Kimura T 2014 *Appl. Phys. Lett.* **104** 022907
- [20] Kocsis V et al 2019 *Nat. Commun.* **10** 1247
- [21] Sergienko I A and Dagaotto E 2006 *Phys. Rev. B* **73** 0944343
- [22] Katsura H, Nagaosa N and Balatsky A V 2005 *Phys. Rev. Lett.* **95** 057205
- [23] Choi Y J, Yi H T, Lee S, Huang Q, Kiryukhin V and Cheong S-W 2008 *Phys. Rev. Lett.* **100** 047601
- [24] Zhai K, Shang D-S, Chai Y-S, Li G, Cai J-W, Shen B-G and Sun Y 2018 *Adv. Funct. Mater.* **28** 1705771
- [25] Tokunaga Y, Taguchi Y, Arima T and Tokura Y 2012 *Nat. Phys.* **8** 838–44
- [26] Wang Y, Pascut G L, Gao B, Tyson T A, Haule K, Kiryukhin V and Cheong S-W 2015 *Sci. Rep.* **5** 12268
- [27] Oh Y S, Artyukhin S, Yang J J, Zapf V, Kim J W, Vanderbilt D and Cheong S-W 2014 *Nat. Commun.* **5** 3201
- [28] Kimura T 2012 *Annu. Rev. Condens. Matter Phys.* **3** 93–110
- [29] Pullar R C 2012 *Prog. Mater. Sci.* **57** 1191–334
- [30] Tokunaga Y, Kaneko Y, Okuyama D, Ishiwata S, Arima T, Wakimoto S, Kakurai K, Taguchi Y and Tokura Y 2010 *Phys. Rev. Lett.* **105** 257201
- [31] Kimura T, Lawes G and Ramirez A P 2005 *Phys. Rev. Lett.* **94** 137201
- [32] Kitagawa Y, Hiraoka Y, Honda T, Ishikura T, Nakamura H and Kimura T 2010 *Nat. Mater.* **9** 797–802
- [33] Okumura K, Ishikura T, Soda M, Asaka T, Nakamura H, Wakabayashi Y and Kimura T 2011 *Appl. Phys. Lett.* **98** 212504
- [34] Chun S H et al 2012 *Phys. Rev. Lett.* **108** 177201
- [35] Chai Y S, Chun S H, Cong J Z and Kim K H 2018 *Phys. Rev. B* **98** 104416
- [36] Shen S-P et al 2017 *Phys. Rev. B* **95** 094405
- [37] Nakajima T, Tokunaga Y, Matsuda M, Dissanayake S, Fernandez-Baca J, Kakurai K, Taguchi Y, Tokura Y and Arima T 2016 *Phys. Rev. B* **94** 195154
- [38] Lee H B, Song Y-S, Chung J-H, Chun S H, Chai Y S, Kim K H, Reehuis M, Prokeš K and Mat'áš S 2011 *Phys. Rev. B* **83** 144425